

An anisotropic numerical model for thermal hydraulic analyses: application to liquid metal flow in fuel assemblies

F Vitillo, D Vitale Di Maio, C Galati, G Caruso¹

“Sapienza” University of Rome – Dep. of Astronautical, Electrical and Energy Engineering (DIAEE) – Corso Vittorio Emanuele II, 244 – 00186 Rome, IT

E-mail: gianfranco.caruso@uniroma1.it

Abstract. A CFD analysis has been carried out to study the thermal-hydraulic behavior of liquid metal coolant in a fuel assembly of triangular lattice. In order to obtain fast and accurate results, the isotropic two-equation RANS approach is often used in nuclear engineering applications. A different approach is provided by Non-Linear Eddy Viscosity Models (NLEVM), which try to take into account anisotropic effects by a nonlinear formulation of the Reynolds stress tensor. This approach is very promising, as it results in a very good numerical behavior and in a potentially better fluid flow description than classical isotropic models. An Anisotropic Shear Stress Transport (ASST) model, implemented into a commercial software, has been applied in previous studies, showing very trustful results for a large variety of flows and applications. In the paper, the ASST model has been used to perform an analysis of the fluid flow inside the fuel assembly of the ALFRED lead cooled fast reactor. Then, a comparison between the results of wall-resolved conjugated heat transfer computations and the results of a decoupled analysis using a suitable thermal wall-function previously implemented into the solver has been performed and presented.

1. Introduction

In order to obtain fast and accurate results, the isotropic eddy-viscosity RANS approach is often used in nuclear engineering applications: in particular, the $k-\varepsilon$ model, $k-\omega$ model and SST model are examples of isotropic two-equations models widely used. As known from the literature, these models can fail when dealing with complex flows, especially when secondary flows are important. Another approach is then provided by Reynolds Stress Models (RSM), in which all the components of the Reynolds stress tensor are directly computed: this makes them suitable for anisotropic flows treatment but, as main drawback, it requires an expensive computational effort and potentially suffers numerical stability problems.

A different approach is provided by Non-Linear Eddy Viscosity Models (NLEVM), which try to take into account anisotropic effects by a nonlinear formulation of the Reynolds stress tensor. This approach is very promising, as it results in a very good numerical behaviour and in a potentially better fluid flow description if compared with classical isotropic models. An Anisotropic Shear Stress Transport (ASST) model, developed in a previous study [1] and implemented into the commercial software ANSYS FLUENT®, has been applied showing very trustful results for a large variety of flows and applications.

¹ To whom any correspondence should be addressed.

As liquid metals do not meet the so-called Reynolds analogy (which assumes a complete similarity between the momentum and the thermal boundary layers via the use of the turbulent Prandtl number close to one), a suitable expression for the turbulent Prandtl number has been implemented into the solver; it allows at performing a complete thermal-hydraulic analysis using the Simple Gradient Diffusion Hypothesis to model the turbulent heat flux. A comparison between the results of wall-resolved conjugated heat transfer computations and the results of a decoupled analysis using a suitable thermal wall-function which had been previously implemented into the solver has been performed and presented [2].

In the present paper, a CFD study focused on the application of the abovementioned approaches has been carried out on the liquid metal flow within the fuel assembly of the ALFRED lead cooled fast reactor.

2. Wall function approach

To be able to keep a Simple Gradient Diffusion Hypothesis in our analysis and to take into account the enhanced heat transfer in liquid metals (due to their high thermal conductivity) a new correlation to link turbulent viscosity to turbulent heat diffusivity by means of the turbulent Prandtl number ($Pr_t = \nu_t / \alpha_t$) is needed. The needing of assessment is evidenced by the numerous correlations proposed in the past through experimental campaigns or analytical studies. Among them, the model of Kays [3] provides very good results [2]:

$$Pr_t = 0.85 + \frac{0.7}{Pr} \frac{\nu}{\nu_t} \quad (1)$$

In the wall-resolved approach the first node along the y axis need to be positioned in such a way that $y_1^+ \leq 1$, leading to very time-consuming simulations, because this method devotes a substantial fraction of the whole computational time to the near wall region, where velocity and temperature profiles are steep due to viscous effects.

The wall function approach, on the contrary, allows at using a more uniform mesh with y_1^+ greater than one and using semi empirical formulas to link the viscosity affected region between the wall and the fully-turbulent region.

These functions are based on the universal linear and log laws for velocity; the conventional temperature wall functions have been built for conventional fluids (air, water) and hence they depend on the velocity field according to the Reynolds analogy. Since no logarithmic law is visible in the temperature profile dealing with liquid metals, a new wall function has to be used.

The law proposed by Bricteux et al. [4] as temperature wall function in liquid metals is:

$$\theta^+ = \frac{Pr_t}{\kappa} \log \left(1 + \frac{\kappa}{Pr_t} Pr y^+ \right) \quad (2)$$

DNS and LES data, for a range of Péclet numbers ($Pr=0.025-0.01$ and $Re_\tau=180-2000$), were compared with this law showing a good agreement in the range $y^+=70-300$, where the logarithmic law for the velocity profile is applicable.

Since ANSYS FLUENT does not allow the user to define an user wall function (UDF) for the temperature field, a strategy to overcome this limit has been previously proposed and consists in a step-by-step solution of the flow field, as explained below [2].

First, the velocity field is computed using the enhanced wall treatment. Once the solution is converged, a user defined wall function for the velocity is hooked up in the solver, while are freezed the resolution of the momentum and turbulence equations and is activated the resolution of the energy transport equation. When the calculation is run again, the user defined wall function will not affect the velocity field, but it will be used by the solver to compute the temperature field near the wall.

Few iterations (i.e. five or six), alternating the enhanced wall treatment and the user wall function computations, in which the energy and the momentum and turbulence equations are alternatively

frozen, are needed to quickly obtain a converged solution with temperature-dependent thermo-physical properties, as in the present analyzed case.

The UDF employed is based on the pre-existing standard wall functions (since these wall functions are replaced by the new one). Let's consider the temperature wall function as a linear variation of the velocity one:

$$T^* = \begin{cases} Pr_t y^* = Pr_t U^* & \text{for } y^* < y_t^* \\ Pr_t \left[\frac{1}{\kappa} \ln(Ey^*) + P \right] = Pr_t [U^* + P] & \text{for } y^* > y_t^* \end{cases} \quad (3)$$

Where y_t^* is the thermal sub-layer thickness. Since the first y^* is such as it is outside of the thermal sub-layer (i.e. in the velocity logarithmic sub-layer), only the second law is applied (i.e. for $y^* > y_t^*$). Thus, remembering that in the log-region it holds $U^* = \frac{1}{\kappa} \ln(Ey^*)$, it results that:

$$T^* = \frac{(T_w - T_p) \rho c_p C_\mu^{0.25} k_p^{0.5}}{q_w} = Pr_t [U^* + P] \quad (4)$$

It can be imposed:

$$Pr_t [U^* + P] = T^* = \theta^+ \frac{C_\mu^{0.25} k_p^{0.5}}{u_\tau} = \frac{C_\mu^{0.25} k_p^{0.5}}{u_\tau} \cdot \frac{Pr_t}{\kappa} \log \left(1 + \frac{\kappa}{Pr_t} Pr_t y^+ \right) \quad (5)$$

Thus, defining:

$$U^* = \frac{C_\mu^{0.25} k_p^{0.5}}{u_\tau} \cdot \frac{1}{\kappa} \log \left(1 + \frac{\kappa}{Pr_t} Pr_t y^+ \right) - P \quad (6)$$

And setting a value for Pr_t at the wall, one can have:

$$T^* = Pr_t \left[\frac{C_\mu^{0.25} k_p^{0.5}}{u_\tau} \cdot \frac{1}{\kappa} \log \left(1 + \frac{\kappa}{Pr_t} Pr_t y^+ \right) \right] \quad (7)$$

$$\Rightarrow \theta^+ = \frac{(T_w - T_p) c_p \rho u_\tau}{q_w} = \frac{u_\tau T^*}{C_\mu^{0.25} k_p^{0.5}} = \frac{Pr_t}{\kappa} \log \left(1 + \frac{\kappa}{Pr_t} Pr_t y^+ \right) \quad (8)$$

as required from Eq. (2). The new temperature wall function is employed in a Realizable k - ε model [5] simulation.

3. A non-linear eddy viscosity model: the ASST model

Non-linear eddy viscosity (NLEV) models offer a potentially powerful solution to improve numerical model ability to describe anisotropic characteristics of complex flows. In particular they are supposed to be capable of better predicting secondary motion magnitude as well as flow turbulent features. The Anisotropic Shear Stress Transport (ASST) model has been developed and implemented into the solver ANSYS FLUENT via User-Defined Functions. The model is based on a second-order formulation of the Reynolds stress tensor, written according to the Cayley-Hamilton theorem as follows:

$$\begin{aligned} \overline{\rho u_i' u_j'} = & \frac{2}{3} \rho k - \mu_t S_{ij} + \rho C_1 k \tau^2 \left(S_{ik} S_{kj} - \frac{1}{3} \delta_{ij} S_{kl} S_{kl} \right) + \rho C_2 k \tau^2 (\Omega_{ik} S_{kj} + \Omega_{jk} S_{ki}) \\ & + \rho C_3 k \tau^2 \left(\Omega_{ik} \Omega_{kj} - \frac{1}{3} \delta_{ij} \Omega_{kl} \Omega_{kl} \right) \end{aligned} \quad (9)$$

$S_{ij} = \left(\frac{\partial u_i}{\partial x_j} + \frac{\partial u_j}{\partial x_i} \right)$ being the strain tensor, $\Omega_{ij} = \left(\frac{\partial u_i}{\partial x_j} - \frac{\partial u_j}{\partial x_i} \right)$ being the rotation tensor, k being the turbulent kinetic energy and ω the specific dissipation rate. τ is the turbulent time scale, which, for an ω -based model is typically equal $\tau = \frac{1}{\beta^* \omega}$, with $\beta^* = 0.09$.

The model uses the k - ω transport equations of the well-known SST model of Menter [6]. However a modification of the eddy viscosity formulation is necessary to take into account the Bradshaw's assumption inside the boundary layer and the new anisotropic formulation of the Reynolds stresses. The proposed expression for the eddy viscosity is then:

$$\mu_t = \frac{\rho B}{\max\left[\frac{B}{C_{\mu k} F_2 S}\right]} \quad (10)$$

Where $C_{\mu} = \frac{7.4}{A_1 + \tau S}$, $B = (a_1 + C_1 \tau^2 S^2 + C_2 \tau^2 S^2 + C_3 \tau^2 S^2) \cdot k$ and $S = \left(\frac{1}{2} S_{ij} S_{ij} \right)^{1/2}$. Closure coefficients are $A_1=3.9$ and $a_1=0.31$.

The model is fully realizable thanks to some constraints on the closure coefficients. In particular, retaining the same approach presented in literature [7] and [8], the following relations must hold:

$$C_1 = \frac{C_{NL1}}{C_{NL4} + C_{NL5} \cdot (\tau S)^3} \quad (11)$$

$$C_2 = \frac{C_{NL2}}{C_{NL4} + C_{NL5} \cdot (\tau S)^3} \quad (12)$$

$$C_3 = \frac{C_{NL3}}{C_{NL4} + C_{NL5} \cdot (\tau S)^3} \quad (13)$$

Reference values [8] are used for all the constants, i.e. $C_{NL1}=0.8$, $C_{NL2}=11$, $C_{NL3}=4.5$, $C_{NL4}=1000$ and $C_{NL5}=1$. The C_{NL2} value is of particular interest for a rod bundle flow analysis since it allows improved predictions of secondary motions in this kind of flow [8].

The model is closed through the SST k and ω transport equations [6]:

$$\begin{aligned} \frac{\partial}{\partial t}(\rho k) + \frac{\partial}{\partial x_j}(\rho k u_j) &= \frac{\partial}{\partial x_j} \left[\left(\mu + \frac{\mu_t}{\sigma_k} \right) \frac{\partial k}{\partial x_j} \right] + \\ &+ \widetilde{G}_k - \rho \beta^* k \omega \end{aligned} \quad (14)$$

$$\begin{aligned} \frac{\partial}{\partial t}(\rho \omega) + \frac{\partial}{\partial x_j}(\rho \omega u_j) &= \frac{\partial}{\partial x_j} \left[\left(\mu + \frac{\mu_t}{\sigma_\omega} \right) \frac{\partial \omega}{\partial x_j} \right] + \\ &+ G_\omega - \rho \beta \omega^2 + D_\omega \end{aligned} \quad (15)$$

To be consistent with the NLEV formulation, the turbulence kinetic energy production term can be expressed in the proper form:

$$G_k = -\rho \overline{u_i' u_j'} \frac{\partial u_i}{\partial x_j} \quad (16)$$

Where $\overline{u_i' u_j'}$ is given by Eq. (9). Note that, due to the realizability condition given by the eddy viscosity modification and the model coefficient expressions, no turbulence kinetic energy production limiter is needed. Finally the specific dissipation rate is expressed in the original form i.e.

$$G_\omega = \frac{\rho \alpha}{\mu_t} G_k \quad (17)$$

The other parameters not mentioned so far maintains the same definition as the original SST model formulation. Closure constants are:

$$\begin{aligned} \sigma_{k,1} &= 1.176, & \sigma_{k,2} &= 1.0, & \sigma_{\omega,1} &= 2.0, & \sigma_{\omega,2} &= 1.168, \\ \beta^* &= 0.09, & a_1 &= 0.31, & \beta_{i,1} &= 0.075, & \beta_{i,2} &= 0.0828 \end{aligned}$$

4. The ALFRED core and nodalization

The simulations performed are based on the ALFRED (Advanced Lead Fast Reactor European Demonstrator) triangular core lattice geometry. This lead cooled reactor is the third considered within the LEADER (Lead - cooled European Advanced DEMonstration Reactor) project, and is thought to be realized in the short term, relying on presently available technology. This scaled down reactor is thus designed using solutions close to the lead fast reactor reference conceptual design as much as possible, but still considering the essential need to proceed to construction in a short time frame. Many design details of this reactor can be found in [9]; the main parameters are reported in Table 1.

Table 1. ALFRED core parameters.

Parameter (Core)	Value	Unit	Parameter (Fuel pin)	Value	Unit
Thermal power	300	MW _{th}	Cladding material	15 - 15 Ti	-
Coolant mass flow rate	25460	kg/s	Clad rugosity	$5 \cdot 10^{-6}$	m
Coolant average velocity, \bar{u}	1.4	m/s	Relative rugosity, ε	$5.17 \cdot 10^{-4}$	-
Number of FAs/Total assemblies	171/295	-	Cladding outer radius, r	$5.25 \cdot 10^{-3}$	m
Pins per fuel assembly	127	-	Pitch to diameter ratio, p/D	1.32	-
Coolant inlet temperature, T _{in}	400	°C	Hydraulic diameter, D _h	0.009673	m
Coolant outlet temperature, T _{out}	480	°C	Total length/ Active height	1.42/0.6	m

The central assembly power is 2.063 MW and the maximum heat flux in the central fuel assembly is $9.92 \cdot 10^5$ W/m²; these values have been estimated considering the radial and axial peak factors, 1.2 and 1.209 respectively, and the extrapolated length equal to 150% of the active length. The average flow rate in the central assembly is 176.5 kg/s, with a FA inlet velocity of 1.54 m/s. A bypass flow of 0.373 kg/s associated to each FA (1.7 kW of thermal power in each FA bypass) has been considered.

In the near-wall approach, the estimation of the y_l^+ is crucial to create the mesh to employ.

As known, the requirement to be fulfilled is $y_l^+ < 1$, thus:

$$y_l^+ = \frac{y u_\tau \rho}{\mu} < 1 \quad (18)$$

For the geometry described in Table 1, a preliminary evaluation of the flow field in the active zone provided that the condition $y_l^+ = 1$ will be satisfied with distances from the wall in the range 2.22 μ m and 2.6 μ m. The domain used in the simulations consists of 1/12 of the fuel element 1 m long (composed by the asset length of 0.3 m at the inlet (more than 30 equivalent diameters), 0.6 m for the active length and 0.1 m in the upper zone).

A sensitivity analysis on the nodalization to be used in the near-wall approach and the ASST model has been performed, by using two different boundary layers, $y_l^+ = 1$ (Case A) and $y_l^+ = 0.5$ (Cases B and C), for 16 and 18 layers with a growth rate (which is the ratio of a layer's height and the previous one) equal to 1.3 and two geometrical elements (tetraedrical – Cases A and C - and hexaedrical elements – Case B). The axial size of the mesh is 5 mm for the whole length of the fuel element. Table 2 summarizes the mesh sensitivity and the total number of nodes. Due to the negligible differences in the results obtained with the A, B and C nodalizations, mainly the Cases B and D will be discussed in the paper.

For the wall function approach, a coarser hexaedrical mesh has been prepared, without boundary layer and a $y_l^+ = 170$ (Case D), with the same axial discretization as in the previous cases.

Table 2. Nodalization of the computational domain

Case	Elements type	y_l^+	Approach	Number of nodes
A	Tetra	1	Wall resolved	≈ 2.6 M
B	Hexa	0.5	Wall resolved	≈ 3.5 M
C	Tetra	0.5	Wall resolved	≈ 2.9 M
D	Hexa	170	User Wall function	≈ 0.8 M

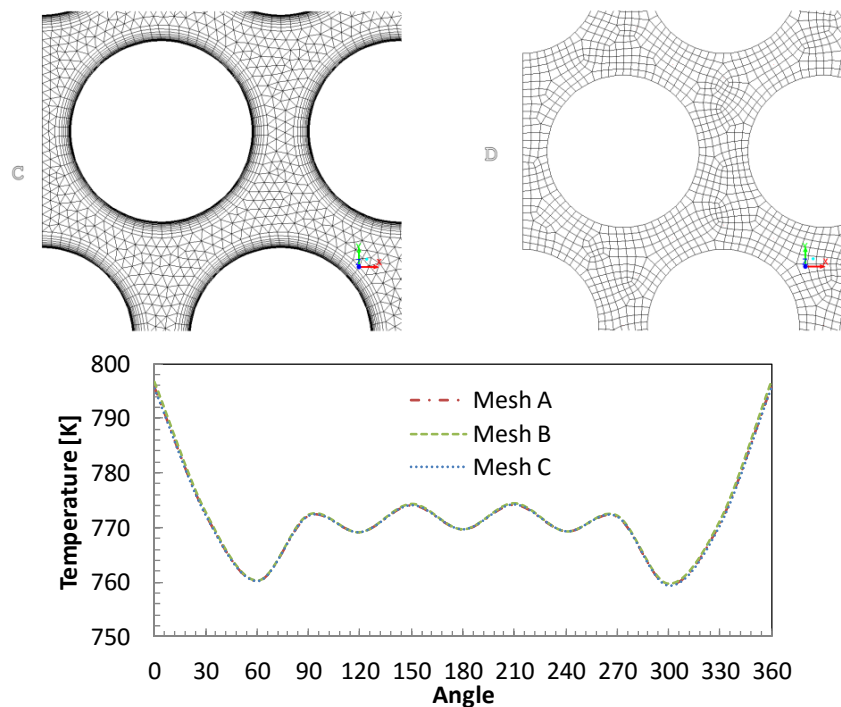


Figure 1. Domain nodalizations and convergence test

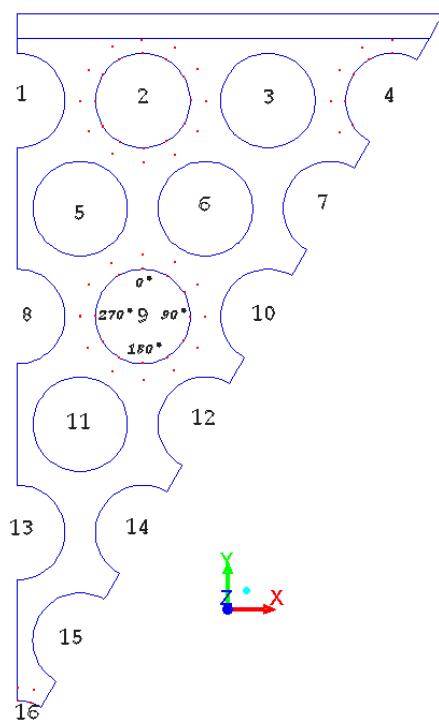


Figure 2. Geometry (transversal section of the 1/12 FA) and temperature lines location

An example of the analyzed nodalizations is shown in Figure 1, where case C and D of Table 2 are shown. Also, an example of the mesh convergence tests for the three wall-resolved configurations is given in the same figure for the angular wall temperature distribution in pin #2.

The domain includes 16 pins, as shown in Figure 2, where the pins are numbered for reference with respect to the result presentation and discussion. In the same figure the positions of the axial lines where pin wall and fluid temperatures were extracted (to evaluate their axial and circumferential profiles) are evidenced. With reference each fluid and wall temperatures couple, the Nusselt numbers have been evaluated from locally imposed the heat flux, the hydraulic diameter and the temperature-dependent thermal conductivity of lead. The distance of the fluid temperature line from the corresponding wall temperature one is half of the minimum distance between pins ($0.16 d_{pin} = 1.68 \text{ mm} \approx 650 y^+$).

5. Results and discussion

First of all it is of primary importance to verify that the used models are able to correctly reproduce the main features of the triangular lattice flow. In this sense, observe in Figure 3 and Figure 4 the velocity and temperature field respectively calculated by the realizable $k-\varepsilon$ model with wall-resolved (WR, with mesh B) and wall-function (WF, with mesh D) approaches.

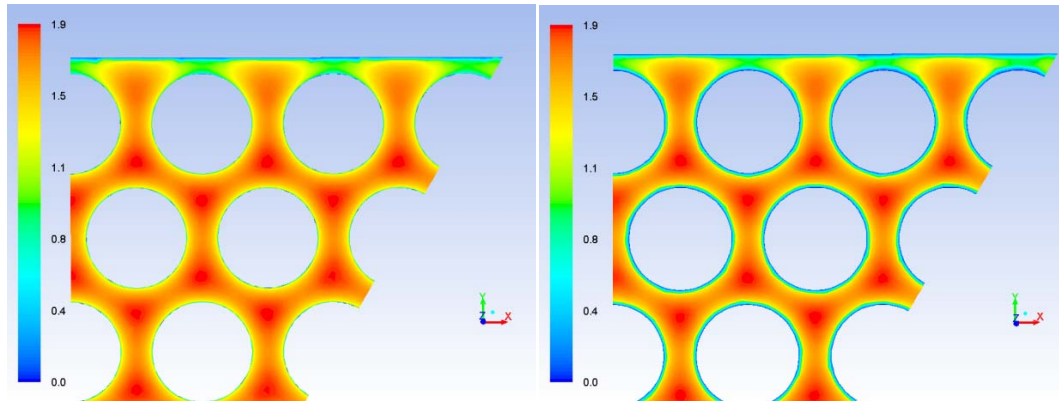


Figure 3. Axial velocity field for a Realizable $k-\varepsilon$ wall-resolved simulation (on the left) and for a $k-\varepsilon$ simulation using the new temperature wall function (on the right) [m/s]

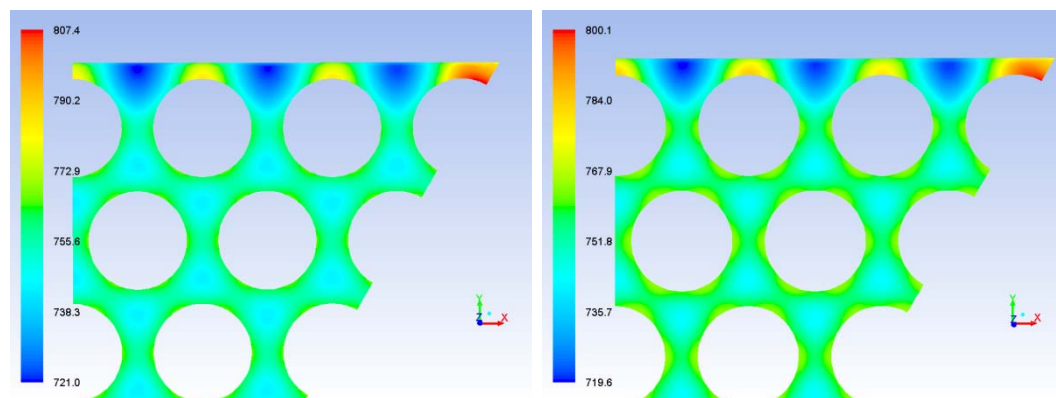


Figure 4. Axial temperature field for a Realizable $k-\varepsilon$ wall-resolved simulation (on the left) and for a $k-\varepsilon$ simulation using the new temperature wall function (on the right) [K]

The two different approaches provide very similar results, both qualitatively and quantitatively. The velocity field presents a peak in the region where hydraulic resistance is lower (i.e. in the central region of the triangular lattice). The main differences between the two approaches are mainly located in the boundary layer region, which is what it is expected due to the different near-wall approach. In particular, the momentum boundary layer is thicker in the $k-\varepsilon$ wall-function computation than in the Realizable $k-\varepsilon$ wall-resolved case. This is quite interesting, since the standard wall functions for velocity are developed for a one-dimensional flow when secondary motions are practically negligible compared to the principal motion. This is not the case for rod bundle flow, where secondary motions are responsible for a strong homogenization of the flow inside the different subchannels. Moreover, the observed thicker boundary layer results in a thicker thermal boundary layer as well: the flower-shaped thermal boundary layer is much more pronounced for the wall-function calculations than for the wall-resolved case.

Due to the observed differences, it is important to verify whether the two approaches can reproduce the correct trend of the Nusselt number predicted by the currently used correlations found in the literature, specifically the Ushakov's [10] and Mikityuk's [11] correlations. Note that these correlations are evaluated with respect to the theoretical temperature profile of the coolant. Figure 5

shows the comparison of the computed Nusselt number as a function of core elevation (centered in the center of the active core height), with that obtained using the two aforementioned correlations, for the 0° position in pin #9 and #16. The same comparison has been also done on the angular distribution of the Nusselt number for pin #9 at the middle point of the active core height. These two pins #9 and #16 are supposed to be the more appropriate to be compared to the experimental correlations, since the effects of the assembly shroud are lower and the fluid flow is closer to the theoretical flow inside an infinite triangular lattice geometry. Note that the quite constant value of the Nusselt number obtained through correlations is used, since it is evaluated by means of the local non-dimensional numbers of the studied case (taking into account the limited effects of the lead temperature variation on the thermophysical properties). The Mikityuk's correlation is presented with its root-mean-squared error bars, trying to quantify eventual differences between numerical and experimental data.

All the different tested models and approaches seem to be able to satisfactorily reproduce values of the Nusselt number. In particular, the axial Nusselt number approaches the experimental value once the inlet effects become negligible. The computed Nusselt number varies as function of the angular position (i.e. the already mentioned flower-shape observed in Figure 4), but still the average value remains within the experimental uncertainty of the Mikityuk's correlation. Therefore the straightforward conclusion is that, when dealing with global feature of the fluid flow, commonly used CFD is capable of reproducing the correct trends, no matter the turbulence model used. However, differences are expected when looking at local quantities, (i.e. wall temperature distributions) due to the different type of model and approach to resolve the boundary layer. In this sense, Figure 6 shows the axial evolution of the wall temperature at the 0° position and Figure 7 shows the angular distribution of the wall temperature at the center of the core active length for pin #2 and #9. The pin #9 is used again as the effects of the assembly shroud are negligible, whereas the pin #2 is chosen since it could provide information on the changes induced by the shroud itself.

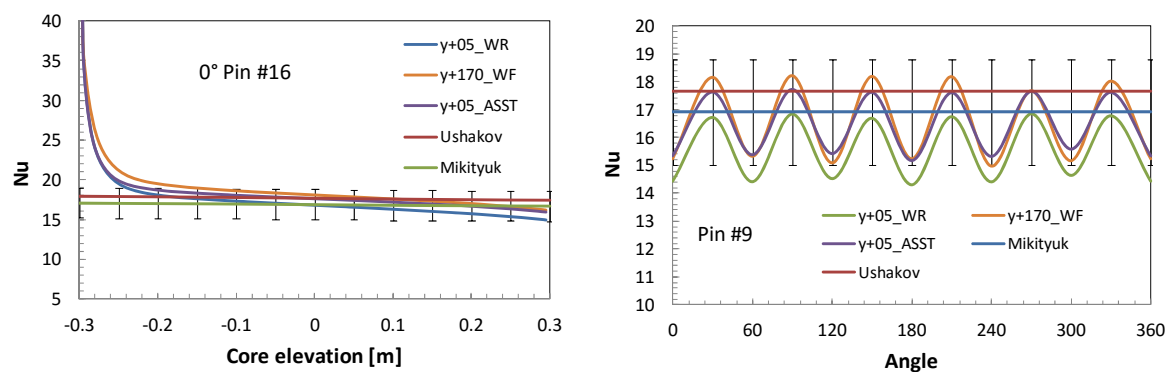


Figure 5. CFD model validation with regard to Nusselt number correlations available in the literature

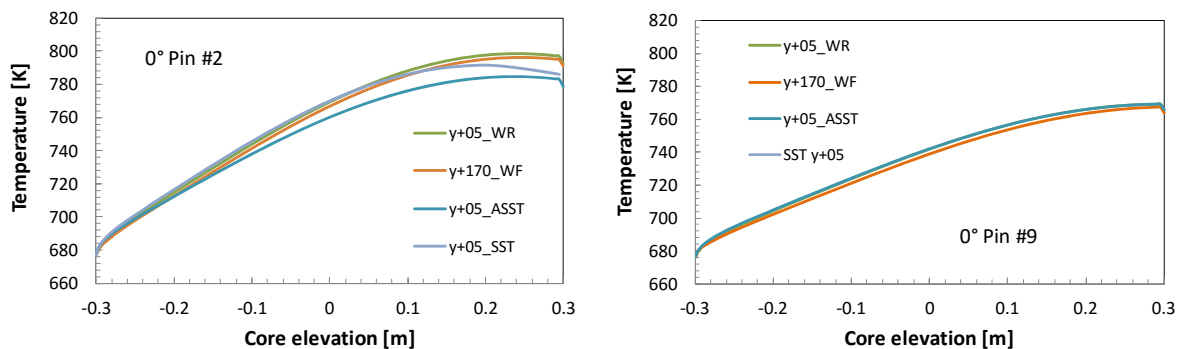


Figure 6. Comparison of the axial wall temperature distribution

As Figure 6 and Figure 7 show, differences do exist: in particular, if the axial wall temperature evolution is practically the same no matter the turbulence model and the near-wall approach used for pin #9, the assembly shroud changes this distribution so that the ASST compute wall temperature at the top of the core active height is 10-15°C lower than that of the $k-\varepsilon$ based calculations. Differences are even clearer when looking at the angular distribution of the pin wall temperature in pin #2 in Figure 7.

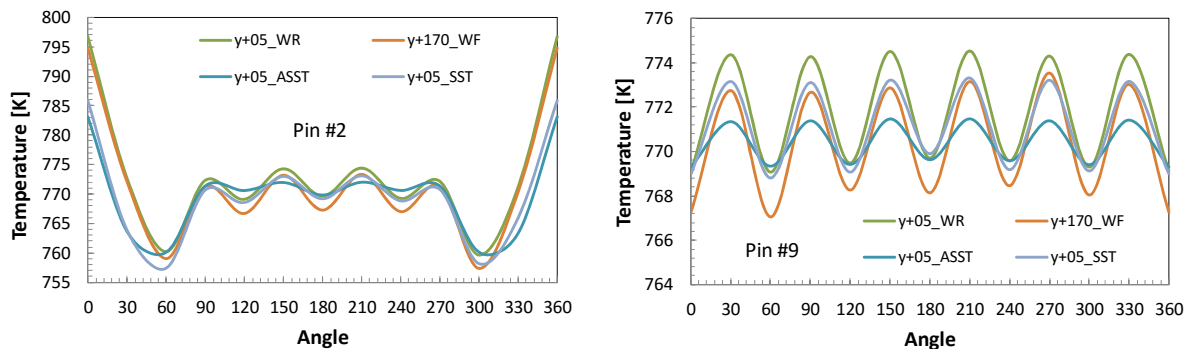


Figure 7. Comparison of the angular wall temperature distribution

Since it could be stated that it is difficult to understand the contribution of the several modeling differences between the wall-resolved ASST results and the wall-function $k-\varepsilon$ results (i.e. the near-wall approach, the dissipation equation, the expression of the Reynolds stress tensor), the results of an isotropic SST [6] calculations are shown as well in Figure 7. This helps a lot the comprehension of the shown comparison, since the SST model employs the same dissipation equation as the ASST model but its isotropic nature is the same as that of the $k-\varepsilon$ model. Therefore, note that when the ω -dissipation equation is used, the wall temperature is underestimated of around 10°C compared to that of a $k-\varepsilon$ simulation (by using either the user defined wall function for temperature with the coarse mesh D or the wall-resolved approach with mesh B) in the region right in front of the assembly shroud (from 270° to 90° in Figure 2).

This difference is likely due to the fact that this region presents a mesh with a $y^+ (= 170)$ in the logarithmic region of the boundary layer (for sake of feasibility of the computations with available means). Therefore, for a given imposed solution of the velocity field in the first cell next to the wall, the temperature field is somehow influenced by the turbulence dissipation occurring in such region, which is modeled differently. Remember that the turbulence dissipation equation is a major source of uncertainty in CFD calculations, since no exact equation exist for this kind of quantity. However, difference are much lower on the other side of pin #2 (i.e. 90° to 270°) oriented towards the inner part of the fuel assembly. By the way, observe that the angular fluctuations are practically the same for the isotropic models, whereas the ASST models have a smoother distribution due the effect of anisotropy: in particular, its favorable characteristics of better reproducing secondary motions can enhance the heat transfer mixing among the different subchannels.

The same conclusion is valid for wall temperature angular distribution in pin #9, when the fluctuations around the mean value are of the order of 2-3°C for the isotropic models and of around 0,5°C for the ASST model.

6. Conclusions

A CFD analysis has been carried out to study the thermal-hydraulic behavior of liquid metal coolant in the fuel assembly of triangular lattice of the lead-cooled ALFRED reactor. Different turbulence models (namely the realizable $k-\varepsilon$, the SST and the ASST models) and different near wall approaches (i.e. wall-resolved and wall-functions) have been tested and compared.

Results show that all the tested models and near wall approaches can predict quite well the global flow characteristics: the results are qualitatively the same and quantitatively very similar. In particular, the Nusselt number predicted by all the tested models lies within the experimental uncertainty range of well-known correlations found in the literature (Ushakov's and Mikityuk's correlations). Differences are observed when looking at very local quantities such as the wall temperature. In this case, the isotropic models predict larger spatial fluctuations compared to the ASST model. The former can in fact damp the fluctuations thanks to a better prediction of the inter-subchannel mixing due to secondary motions. The Simple Gradient Diffusion Hypothesis approach for the turbulent heat flux seems to be able to capture the global heat transfer inside the fuel assembly, when a proper correlation for the turbulent Prandtl number is used. This is likely due to the fact that for such flows the Péclet number is low, hence the conduction heat transfer prevails on the convection (i.e. turbulence-driven) heat transfer.

As a conclusion, the tested models and approaches are able to reproduce the main features of the rod-bundle flow and to provide a good first estimation of the flow characteristics. However, they can potentially be untruthful when performing a finer analysis looking at very local quantities. Therefore care must be taken when performing a CFD analysis of such complex flows.

List of Symbols

k	turbulent kinetic energy [m^2/s^2]		
Nu	Nusselt number		
p/D	pitch to diameter ratio		
Pe	Peclet number		
Pr	Prandtl number		
Re	Reynolds number		
T^*	dimensionless temperature		
T_b	bulk temperature [K]		
T_w	channel wall temperature [K]		
u, U	streamwise velocity [m/s]		
u^+, U^*	dimensionless velocity		
u_τ	shear stress velocity [m/s]		
y^+, y^*	dimensionless wall-normal coordinate		
y_l^+	dimensionless first grid point at wall boundary in wall normal direction		
		<i>Greek symbols</i>	
		ε	energy dissipation [m^2/s^3]
		θ	mean transformed temperature [K]
		θ^+	dimensionless θ
		κ	Von Kármán constant
		μ	fluid dynamic viscosity [kg/ms]
		μ_t	fluid turbulent viscosity [kg/ms]
		ν	fluid kinetic viscosity [m^2/s]
		ν_t	turbulent momentum diffusivity [m^2/s]
		ρ	fluid density [kg/m^3]
		τ_w	wall shear stress [kg/ms^2]
		ω	specific energy dissipation [s^{-1}]

References

- [1] Vitillo F, Galati C, Cachon L, Laroche E and Millan P, "An Anisotropic Shear Stress Transport (ASST) Model Formulation", *Comput. Math. Appl.*, <http://dx.doi.org/10.1016/j.camwa.2015.08.023>
- [2] Vodret S, Vitale Di Maio D and Caruso G 2014 *J. Phys.: Conf. Ser.* **547** 012033
- [3] Kays W 1994 *J. Heat Trans.-T. ASME* **2** (116) 284-95
- [4] Bricteux L, Duponcheel M, Winckelmans G, Tiselj I and Bartosiewicz Y 2012 *Nucl. Eng. Des.* **246** 91-97
- [5] Shih T H, Liou W W, Shabbir A, Yang Z and Zhu J 1995 *Comput. Fluids* **24**(3), 227-238
- [6] Menter F R, Kuntz M and Langtry R, "Ten years of industrial experience with the SST Turbulence model", *Turbulence, Heat and Mass Transfer 4*, Begell House, Inc., 2003
- [7] Shih T H, Zhu J and Lumley J L, "A Realizable Reynolds Stress Algebraic Equation Model", NASA TM 105993
- [8] Baglietto E, Ninokata H, and Misawa T 2006 *Nucl. Eng. Des.* **236** 1503-1510
- [9] Grasso G, Petrovich C, Mattioli D, Artioli C, Sciora P, Gugliu D, Bandini G, Bubelis E and Mikityuk K 2014 *Nucl. Eng. Des.* **278** 287-301
- [10] Ushakov P, Zhukov A and Matyukhin M 1977 *High Temp.* **5** (15) 868-73
- [11] Mikityuk K 2009 *Nucl. Eng. Des.* **239** 680-7